Dynamic Power Sharing Assisted Hybrid Controller for PV Fed Isolated dc Microgrid

Arunkumar Chirayarukil Raveendran and Udaya Bhasker Manthati, *Member, IEEE*

***Abstract*—This article presents a hybrid control strategy to improve the control and power sharing of a hybrid energy storage system (HESS) used in an isolated dc microgrid. While the photovoltaic panel is the primary energy source, the battery and supercapacitor work together to meet the additional power requirements. A modification to the traditional filter method for dividing the average and transient HESS current components is done by replacing the low pass filter (LPF) with a rate limiter to ensure proper power splitting and smoother battery discharge. The rate limiter integrates power balance into the system and allows for the integration of battery discharge rates, eliminating the problems caused by the unintentional selection of the cut-off frequency. In addition, the HESS current outputs are no longer affected by low order LPF phase delay. A simple prediction based current control is proposed for HESS current regulation to precisely track the rate-limited current references and avoid common windup concerns associated with proportional integral (PI) controllers arising from system nonlinearities and uncertainties. The proposed control approach can reduce the peak overshoot below 2% and settling time during disturbances less than 15%. Simulation and experimental investigations are carried out to validate the effectiveness of the proposed method.**

***Index Terms*—Battery, dc microgrid, hybrid controller, rate limiter, supercapacitor.**

I. Introduction

ENERGY storage systems play a crucial role in renewable power generation and isolated power supply systems. Of all the energy storage devices, batteries are considered to be the most desirable because of their easy integration with new systems and widely accepted technology [1], [2]. Nevertheless, their comparatively poor power density and considerable internal resistance seriously restrict their power-delivery capabilities under high current loads. Moreover, the battery life is affected by transient currents and high current rates [3]. To overcome these shortcomings, batteries are hybridized with other fast-responsive devices such as supercapacitors (SCs). SCs possess the advantages of high power density, longer life, and high efficiency even though they have relatively low energy density [4]. The complementary features of batteries and SCs enable this combination to function as an optimal energy storage system with integrated features to meet various power requirements. Hence, the combination is termed a hybrid energy storage system (HESS) [5], [6].

In a dc microgrid, the primary functions of HESS include: 1) as a backup source for uninterrupted load power requirements in the event of a power outage; 2) to create backup storage capacity by storing energy during peak hours and returning it to the system during peak load demand; and 3) to improve power quality by facilitating possible fluctuations and uncertainty in supply energy resources such as solar photovoltaics (PVs) [7]–[9]. Different HESS configurations can be integrated with the microgrid. The passive topology with directly connected energy storage devices and semiactive topology with controlled and uncontrolled energy storage devices are used to mitigate the impact of dc bus voltage changes [10], [11]. Although, the total losses in such microgrid topologies are reduced by eliminating additional power converters, the absence of control of the passively linked storage units impedes the effective utilization of its total capacity. In addition, it leads to deficient transient power sharing between the storage units [12].

Extensive ongoing research is mostly on fully active topology integrated microgrid systems to increase storage device utilization and power sharing [13], [14]. A traditional approach to controlling the battery and SC in HESS is the use of proportional integral (PI) controllers [15]. The PI-based HESS controllers mainly use filter methods to assign the average and transient power to the battery and SC, respectively [16], [17]. Authors in [18]–[20], have presented different PI-filter controller configurations for HESS by considering the state of charge (SOC) of battery and SC, dc bus voltage regulation, operation under different microgrid modes, and additional services. These methods use a low order low pass filter (LPF) and a minimum of three PI controllers to isolate the high and low frequency current components of the HESS current reference. The increase in the number of PI controllers requires more parameters to be tuned simultaneously, making the design more complex. Further complexities arise in the design process due to the lack of a systematic approach in determining the cut-off frequency. In fact, the performance of the microgrid system is dependent on the cut-off frequency, which is selected based on the charge-discharge rates of the battery and transient power requirement, rather than the frequency of the power demand. In addition, the lag of LPF and PI controller results in considerable delay in response and poor current regulation of the HESS system [21]–[22].

Some researchers have introduced advanced control algorithms into HESS integrated microgrid systems to address the

Manuscript received 29 October 2021; revised 6 April 2022 and 14 June 2022; accepted 27 July 2022. Date of publication 16 August 2022; date of current version 24 February 2023. *(Corresponding author: Arunkumar Chirayarukil Raveendran.)*

The authors are with the Department of Electrical Engineering, National Institute of Technology, Warangal, Telangana 506004, India (e-mail: acr_research@student.nitw.ac.in; ub@nitw.ac.in).

Digital Object Identifier 10.1109/JSYST.2022.3195812

above shortfalls. A deadbeat control based PV-dc microgrid with HESS is presented in [22]. The system determines the duty pulses in a single iteration. The usage of a LPF combined with the prediction results in a delay in the current reference generation affecting the dynamics of dc bus voltage. In [23] and[24], model predictive control (MPC) strategies are employed to regulate the HESS current and voltage values. The MPC schemes show better results than traditional methods, and rather they require accurate modeling and optimization of the duty based on HESS current. Hence, it requires high-end processors and computational effort for its implementation. The combination of different control schemes are proposed for HESS in [25]–[28]. In [25], the HESS currents are regulated by using a sliding mode controller (SMC), and the PI controller regulates the dc grid voltage. However, the LPF-based power splitting strategy reduces the advantage of using SMC and introduces a delay in reference current calculation. In [26], a nonlinear disturbance observer is added to enhance the performance of the fuel cell—battery—SC system. All the above SMC-based controllers require complex mathematical design procedures, and the system performance depends on the selection of sliding surface. The fuzzy logic controller is used in the HESS control algorithm and is ofttimes integrated with other controllers [27], [28]. A major drawback of fuzzy logic control systems is that they rely totally on human skills and understanding, and the rules of a fuzzy logic system must be updated regularly. A hybrid controller combining damping and the MPC presented in [29] improves the system performance compared to the traditional PI method, and the rate limiter-based controller helps to eliminate system delays. However, it requires complex modeling and optimization to control the dc microgrid.

A two-level hybrid controller with internal predictive control and external PI voltage control is proposed in this article. The proposed duty calculation control of converters relies on basic modeling equations and generates the control signals in one iteration. This helps to reduce the computational burden and enables fast settling of dc bus voltage. The coordinate operation of predictive control and PI control depends on the power sharing between battery and SC. The rate limit unit is introduced to split the current components using a more explicit term that directly indicates the permissible battery charge-discharge rates and eliminates the lagging behavior in LPFs. Furthermore, the combination of duty calculation with the rate limiter ensures rapid dynamic response of the SC while effectively achieving proper reference tracking on slow dynamic battery current. An additional controller is added to the system as a permanent solution for charging of SC. Unlike many other SC charging schemes, the proposed method does not affect the dc bus voltage regulation and charge-discharge rate of battery current. The dc microgrid system is simulated and tested experimentally with various source and load variations to test the effectiveness of the proposed architecture.

The essential contributions of this work are as follows.

1) An improved two-stage hybrid controller with a rate limiter for HESS power decoupling in PV dc microgrid is proposed in this work. The discrete nature of modulating signal calculation enables faster dynamics, and the rate limiter provides controlled decoupling of HESS reference current.
2) A simple SC charging method is implemented for the regulation of SC voltage. The proposed method charges the SC without affecting the dc bus voltage and rate of change of battery current.
3) In addition, the proposed rate limiter-based power decoupling method balances the dc bus power in a single iteration. Hence, it reduces the delay imposed by the LPF on the control loop and reduces the burden in computation.
4) Unlike a battery, the reduction in SC voltage results in the ringing of dc bus voltage. The proposed control method mitigates the ringing in the dc bus and battery when operating under low SC voltage.
5) The proposed system mitigates the effect of variation in PV generation and load demand effectively with minimal voltage variation and settling time.

This article has been organized as follows. Section II discusses the configuration and control of PV-dc microgrid. Section III discusses the proposed HESS power sharing and control strategy for HESS. Section IV shows the simulation results and case studies using MATLAB/Simulink. In Section V, hardware results are presented to validate the simulation results. Finally, Section VII concludes the article.

II. Configuration and Control of PV Fed dc Microgrid

The HESS integrated PV fed dc microgrid considered for the study is shown in Fig. 1. dc–dc converters link the PV source, SC, and battery to the dc bus, while the dc loads are connected directly. The PV, battery, SC, and dc bus voltages are represented by V_{pv}, V_{sc}, V_b, and V_0, respectively. The L_{pv}, L_b, and L_{sc} represent the filter inductances of the PV, battery, and SC converters, and the dc bus voltage filter capacitance is C_0. The variables I_b, i_{pv}, and i_{sc} represent the battery, the PV panel, and the SC current. Control switches for power converters are S_1, S_{b1}, S_{b2}, S_{sc1}, and S_{sc2}. The PV panel converter is a unilateral boost converter based on perturb and observe assisted power point tracking (MPPT) control. The energy storage converters in the system possess two-way capabilities to charge or discharge the power accordingly. The main focus of the HESS controller is the regulation of dc bus voltage, proper power sharing inside the HESS and between HESS and PV panel, and regulation of SC voltage and battery SOC. The key responsibilities of the HESS controller include regulation of dc bus voltage, SC voltage, and ensuring proper power distribution within the HESS and between the HESS and the PV panel. As direct control of output variables is impracticable, a two-loop control scheme is designed to get optimum performance from HESS. The feedback variables considered in the system are dc bus voltage, battery current, and SC current. The external voltage controller measures the error in the dc bus voltage relative to the reference voltage and generates the total HESS reference current. The inner predictive current controllers are designed to calculate the optimal duty to reduce the error in the HESS current. The following sections detail the hybrid controller, SC charging, and PV panel MPPT control design and analysis.

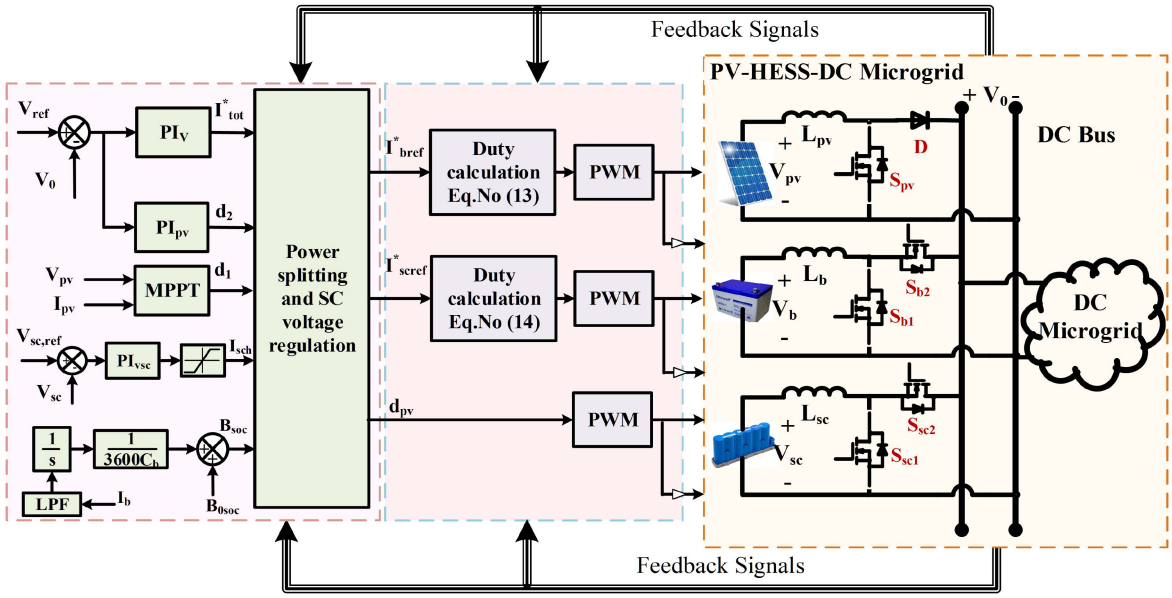

Fig. 1. Configuration of HESS integrated PV fed dc microgrid and control strategy.

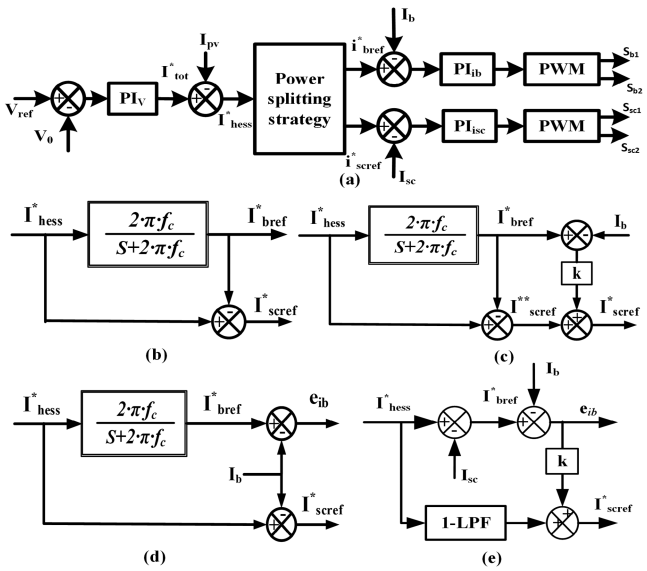

Fig. 2. Traditional PI-LPF based control strategy and its different LPF schemes. (a) Basic two loop control structure. (b) Basic LPF power splitting strategy. (c) Power splitting based on battery current. (d) Power splitting by considering uncompensated battery current. (e) Power splitting based on SC current.

A. Traditional PI-LPF Control Scheme for HESS

The typical HESS control approach requires three PI controllers for load voltage and HESS current regulation. Total current reference values are generated by linearly regulating the dc bus voltage. A detailed description of the conventional control structure and power splitting strategy for HESS current regulation are depicted in Fig. 2. LPFs are used in conjunction with PI controllers to separate the total current reference into steady and transient state current components [15]. A first-order LPF is applied to avoid the impractical complexity of high-order filters in implementation. The LPF decoupling systems choose various cut-off frequencies without a systematic method, with 31 rd/sec being the most commonly picked value [17], which is adopted in this work for comparative analysis. The HESS current reference (i^*_{hess}) is passed through a LPF to generate battery reference current (i_{bref}). The difference between i_{bref} and the i^*_{hess} gives SC current reference as shown in Fig. 2(b). Since PI controllers regulate transient and average current components, poor tracking and windup difficulties occur. A few reference papers [9], [17] worked to improve the power sharing of LPFs by adding uncompensated errors in the system. A simple method is by adding the battery error current to the i_{scref}. Some other control strategies try to generate the reference current by subtracting the actual current from the total current reference, as shown in Fig. 2(d) and (e) [4]. All the above power splitting methods, the inaccuracy in selecting the cut-off frequency, and the slow response of low order LPF degrade the system performance by increasing nonlinearity and slowing system responsiveness.

III. Proposed HESS Power Sharing and Control Strategy

The proposed control strategy combines the simplicity of conventional PI controllers and the fastness of prediction control strategies. It uses the PI control strategy to regulate the load bus voltage. A power splitting-based energy management algorithm is introduced to split the total HESS power demand into the battery and SC reference current. The predictive control calculates the duty signal in a single iteration and reduces the complexity of optimization and tuning. (9) and (10) provide the average model of the converter utilized for bifurcation, whereas (13) and (14) represent the duty calculation, as obtained in Section III-C. Furthermore, a part of the error voltage is added to the HESS current reference to reduce the steady-state error associated with

predictive control. The proposed HESS control system has the following three parts.

1) Generation of HESS current reference from error dc link voltage.
2) A Power management algorithm consists of power balancing and power splitting between battery and SC.
3) Modulating signal calculation utilizing battery and SC inductor currents, as well as a dynamic dc–dc converter model that assures the lowest dc bus voltage.

A. HESS Reference Current Generation

The PV, HESS, and load demand are balanced in the reference current generation stage. PV and HESS must compensate for the load demand. The current reference generation must guarantee that the power supplied by HESS and PV is sufficient to fulfil the load requirement. However, the PV power generation is independent of load demand. Hence, the HES has to balance the power generation and load demand by absorbing or supplying the power from the dc bus. The power balance in the system can be expressed as follows:

$$P_{PV}(t) + P_{\text{bat}}(t) + P_{sc}(t) = P_L(t) = P_{\text{avg}}(t) + P_{tr}(t) \quad (1)$$

where $P_{PV}(t), P_{\text{bat}}(t), P_{sc}(t), P_L(t)$ are the PV power, battery power, SC power, and load power. $P_{\text{avg}}(t)$ and $P_{tr}(t)$ represents the average and transient power exist in the load bus. The total average power is supplied by battery and PV together. The transient power occurs during starting, and disturbances are supplied and absorbed by the SC unit. The total power in the dc bus can be given as follows.

Under steady-state condition

$$P_{\text{bat}}(t) = P_L(t); P_{sc}(t) = 0. \quad (2)$$

The power sharing during SC voltage regulation mode (SC_EN =1) is given by

$$P_{PV}(t) + P_{\text{bat}}(t) = P_L(t) + P_{sc}^{ch}(t) \quad (3)$$

$$P_{sc}^{ch}(t) = -P_{sc}. \quad (4)$$

During charging of SC, $P_{sc}^{ch}(t)$ is positive, and it is negative during $P_{sc}^{ch}(t)$ discharging mode. The $SC\_EN = 1$ is enabled when V_{sc} discharged to lower limits. The battery current reference be written from the power balance equation as

$$i_{bref} = \frac{V_{dc}}{V_b} i_{ref} + i_{sch}. \quad (5)$$

At transient conditions, the discharge of i_{bref} is limited by rate limiter. The rate limiter is designed in such a way that it modifies the i_{bref} based on the previous state. The algorithm used for splitting the total current to steady-state and transient current is shown in Fig. 3, "r" is the charge/discharge limit value of battery current. The $i_{bref}(k+1)$ and $i_{bref}(k)$ are i_{bref} values for the next sampling instant and previous sampling instant, respectively. If the absolute difference between these two is higher than r, then, $i_{bref}(k+1)$ is replaced to

$$i_{bref}(k+1) = i_{bref}(k) \pm r. \quad (6)$$

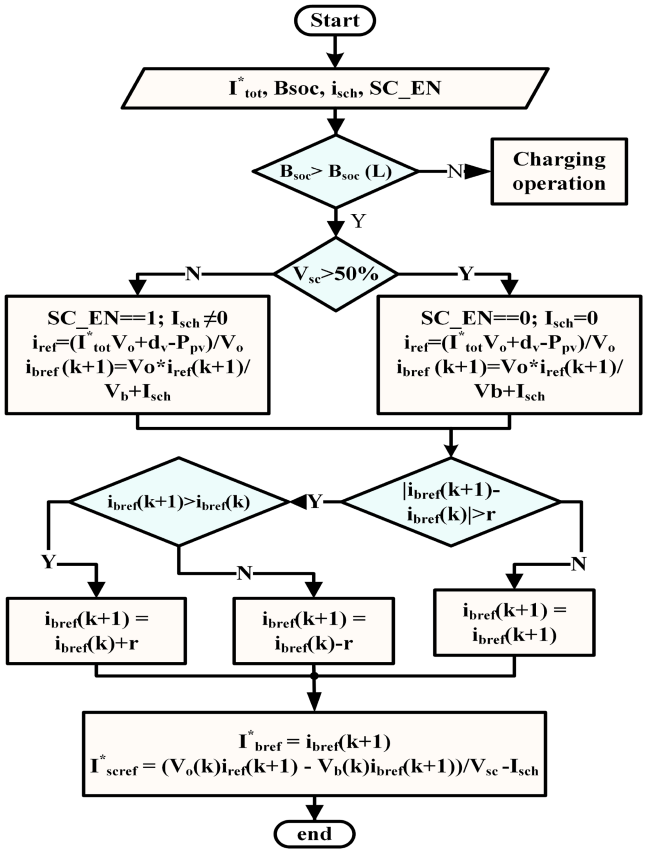

Fig. 3. Schematic representation of rate limiter-based reference current generation by considering SC charging.

The SC should supply the remaining i_{ref} current during this interval to maintain the power balance in the system

$$i_{scref}(k+1) = \frac{i_{ref}(k+1)V_0(k) - V_b(k)i_{bref}(k+1)}{V_{sc}(k)}. \quad (7)$$

B. Voltage Control Design

The outer voltage controller generates the total dc microgrid reference current with respect to the error in dc bus voltage. The right hand plane zero appeared in the boost converter model results in unwanted oscillations in dc bus voltage. Thus, the controller design requires utmost care in the selection of bandwidth for the outer voltage control loop in the case of the PI controller is given as

$$PI_v = K_{pv} + \frac{K_{iv}}{s}. \quad (8)$$

The outer voltage controller generates required current reference from the error in dc bus voltage. The controller generates the complete current reference for the corresponding error. The PI parameters for the outer voltage control loop are designed using the method given in [17]. The phase margin and bandwidth for the outer voltage control loop are selected as 60^0 and 600 rd/sec respectively. The designed values are k_p= 0.25 and k_i= 160.

C. HESS Current Control and Duty Pulse Generation

The average voltage balance equation for inductors is developed to calculate the modulating signals based on reference current, battery, and SC inductor currents. The duty signals are calculated with the help of average model bifurcation using Euler approximation [30]. The averaged equation for L_b is given by

$$\frac{L_b(di_{\text{bat}}(t))}{dt} = V_b(t) - V_0(t)(1 - d_b(t)). \tag{9}$$

For L_{sc}, the current equation is

$$\frac{L_{sc}(di_{sc}(t))}{dt} = V_{sc}(t) - V_0(t)(1 - d_{sc}(t)). \tag{10}$$

After expanding (9) and (10) using Euler's difference law [30]

$$\frac{L_b(i_b(k+1) - i_b(k))}{T_s} = V_{\text{bat}}(k) - V_0(k)(1 - d_b(k)) \tag{11}$$

$$\frac{L_{sc}(i_{sc}(k+1) - i_{sc}(k)}{T_s} = V_{sc}(k) - V_0(k)(1 - d_{sc}(k)). \tag{12}$$

From the perspective of model bifurcation, (11) and (12) can be rearranged to obtain modulating signals d_b and d_{sc}. Also, the $i_{sc}(k+1)$ and $i_b(k+1)$ indicates the reference target for SC and battery current. In other words, the $i_{sc}(k+1)$ and $i_b(k+1)$ can be written as I^*_{scref} and I^*_{bref}. The signals at kth sampling instants indicates the actual measured signals in the system

$$d_b(k+1) = \frac{t_s(V_0(k) - V_b(k)) + L_b(I^*_{bref} - I_b)}{t_s V_0} \tag{13}$$

$$d_{sc}(k+1) = \frac{t_s(V_0(k) - V_{sc}(k)) + L_{sc}(I^*_{scref} - I_{sc})}{t_s V_0}. \tag{14}$$

By comparing d_{bat} and d_{sc} with a sawtooth waveform of period t_s, the duty pulses S_{bat} and S_{sc} can be generated. As a result, the HESS regulates the power demand by their operating characteristics. The prediction-based duty calculation control computes the d_{bat} and d_{sc} in real time within one cycle. That helps the HESS respond quickly to PV and load variations and improves the dynamic performance of the overall system. The overall block diagram of the proposed PI- predictive hybrid controller for HESS is shown in Fig. 1.

D. SC Voltage Control

The SC voltage regulation is achieved by adding a PI controller. The controller is active only when the SC_EN= 1. Unlike a battery, the voltage of a SC can fluctuate from 100% to 0% while operating. Furthermore, 75% of the stored energy in a SC is available at a 100% to 50% voltage range. Further decaying in SC voltage leads to adverse effects on the dc bus [19]. Hence, the lower limit of SC voltage is fixed at 50% as shown in Fig. 3. A simple PI controller generates the charging current reference for SC. The PI will generate the required charging current reference based on the error in SC voltage. The SC charging reference current is added to the total reference current and subtracted from the SC current such that a sudden change in battery current is eliminated. The corresponding total HESS current reference and SC current reference is as follows

$$i_{ref} = \frac{I^*_{tot}V_0(k) + dv(k) - P_{pv}(k)}{V_0(k)} + I_{sch} \tag{15}$$

$$i_{scref}(k+1) = \frac{i_{ref}(k+1)V_{dc}(k) - V_b(k)i_{bref}(k+1)}{V_{sc}(k)} - I_{sch} \tag{16}$$

where $dv(k)$ is the compensating factor added to reduce the steady state error. $dv(k)$ is given by

$$dv(k) = m(V_{ref} - V_0(k)) + dv(k-1). \tag{17}$$

The error constant "m" is a small positive integer chosen to reduce the error in dc bus voltage and helps the HESS current to reach the correct steady-state value.

E. Analysis of Effect of Parameter Variation

The operation of the proposed controller is mainly affected by the duty calculation accuracy and rate limiter constant (r). The rate limiter effect on the battery and SC reference current generation is depicted in Fig. 4(a). The load disturbance considered here is the same for all cases and is applied at 1 s. The required average current is in 6 A. The high "r" value indicates the fast settling of the battery and SC current. As the "r" value decreases, it takes longer for the battery current to reach its final state. Furthermore, the final reaching time depends on the HESS current to be supplied.

The duty calculation depends mainly on the variance in the inductor rather than the capacitor. The variation in calculated battery and SC duties based on variation in inductor values are presented in Fig. 4(b). The calculated duty is higher at lower inductor values, which allows the inductor to store more power. On the other hand, the variance in duty after the specified inductance value is modest, which indicates that the increase in inductance has little effect on the duty calculation. In Fig. 4(c), the variation of calculated duty concerning battery SOC and SC voltage are shown. The dependency of battery duty on battery SOC is minimal and almost constant in the 30%–90% SOC range. On the other hand, the SC duty depends entirely on SC voltage variation. The duty increases as the SC voltage reduces. Below 50% of SC voltage, the duty shows significant increment and saturation at the upper limit. The operation of power converters with a duty above 85% gives rise to other short circuits and thermal issues. Hence, operating SC below 50% of its voltage is not advisable, and charging must be initiated.

IV. Simulation Results and Case Studies

To verify the proposed system, an extensive simulation study is conducted in MATLAB/Simulink. The simulation parameters used for the study are developed based on basic converter modeling given in [31] and the selected parameters are shown in Table I. From Fig. 4, the "r" value is selected as 20 A/sec. The dc microgrid system performance with proposed control structure is verified under the following four scenarios via:

1) increment in PV generation (Scenario-I, at t= t_1);

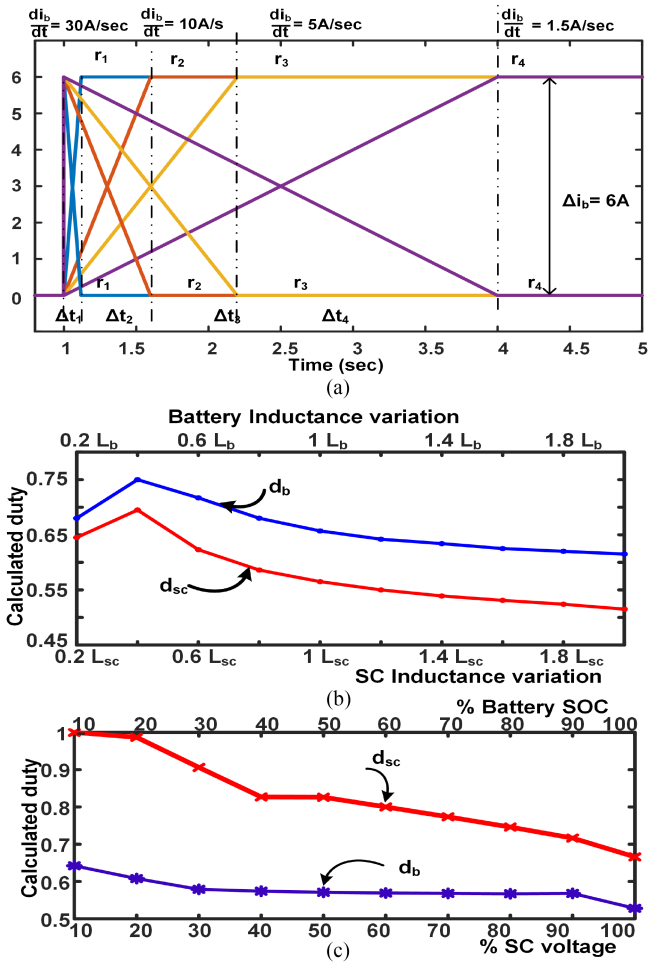

Fig. 4. Analysis of effect of variation in parameters: (a) selection of rate limiter constant and battery rate of discharge, dependency of predicted duty on (b) inductor parameter variation, (c) battery SOC and SC voltage variation.

TABLE I
RATING OF DC MICROGRID COMPONENTS CONSIDERED FOR SIMULATION STUDY

S.No	Parameter	Specifications
1	DC–DC converter	L_{sc}=2.3 mH, L_b=2.3 mH, L_{pv}= 3.25 mH, C_{0dc}= 430 μF
2	Supercapacitor	V_{sc}= 48 V, C_{sc}= 19.3 F
3	PV panel	V_{pv}= 61.4 V, I_{pv}= 16.3s A
4	Output power, P_{out}	1 kW
5	Load voltage, V_0	96 V
6	Switching frequency, f_{sw}	20 kHz

2) decrement in PV generation (Scenario-II, at t= t_2);
3) increment in load demand (Scenario-III, at t= t_3);
4) decrement in load demand (Scenario-IV, at t= t_4).

A. System Operation Under Disturbances

The simulation results are presented for validating the operation system variables at disturbances and power balance among the different devices. The system parameters such as V_0, I_0, I_b, I_{sc}, and I_{pv} under various scenarios are shown in Fig. 5(a). The system power sharing at different instants is shown in Fig. 5(b). Initially, the PV generation and load demand are equal. Therefore, the HESS current is almost zero during this period. At t = t_1, the increase in PV generation from 200 to 450 W causes the injection of extra power to the system. The battery absorbs the excess steady-state power, and the SC absorbs the transient pressure. The load voltage dip (2%) at the time of disturbance and regains its actual value in 7 ms. In conventional control strategies, the rise occurs after the dip. The proposed system is settled before a further rise in voltage. The system regulates the increase in 100% load demand at t = t_3 with reduced load bus variations. From Fig. 5(a), the dc bus voltage is clearly maintained constant at 96 V in all scenarios, with a small variation at the time of disturbance, the change in battery current is slower, and the SC is compensating for the transient current. The total load power demand is shared between the PV, battery, and SC. The SC supplies power only at the time of disturbances that make the SC voltage almost constant during steady state operation, as shown in Fig. 5(b).

B. System Operation Under 50% of SC Voltage

The battery and SC current sharing during Scenario- III with 50% SC voltage is shown in Fig. 6(a). At t = t_1, the load current is increased from 2 to 4 A. The battery current changes to the new state from charging to discharging with a slow rate of change, and the SC delivers the excess power demand. The enlarged portion compares the time taken by load current, battery current, and SC current to reach the final state. With 80% of SC voltage, the dc bus fluctuates nearly 2 V, and with 50 % voltage, the variation in dc bus voltage is 2.5 V. In comparison to the traditional control strategy, the reduction in SC voltage has less impact on dc bus voltage. Furthermore, to verify the charging of SC from the main system, Scenario-III with $SC\_EN = 1$ is considered in Fig. 6(b). Initially, the system is at a steady-state with PV = excess power mode, battery = charging mode, V_0 = 96 V, I_b= –2 A, and I_{sc}= 0 A. At t = 0.5 s, the SC charging is enabled such that battery current change to positive and 1.6% voltage rise occur in the dc bus. Now, the battery is discharging, and the SC is charging. At t = 1.5 s and 2 s, the load disturbances are applied. The maximum peak overshoot at the time of disturbance is 2.1%, and the SC acts quickly to mitigate the transient power. The increase in overshoot is due to the operation of dc microgrid with low SC voltage. It can be seen that the change in battery current is slow during charging and disturbance, which is important for battery life enhancement. Furthermore, the battery and SC react faster, resulting in reduced dc bus voltage oscillations.

C. System Operation With Variation in Rate Limiter Constant

Further simulation studies are conducted to examine the system's performance with variation in the "r" value. Fig. 7(a) shows the load voltage, battery current, and SC current variation with the decrease in "r" value and with a LPF of 31 rd/sec for the same hybrid controller. The rate limiter-based method shows that it limits the overdischarge of the battery compared to the LPF. Further, the "r" allows the designer to select the battery's

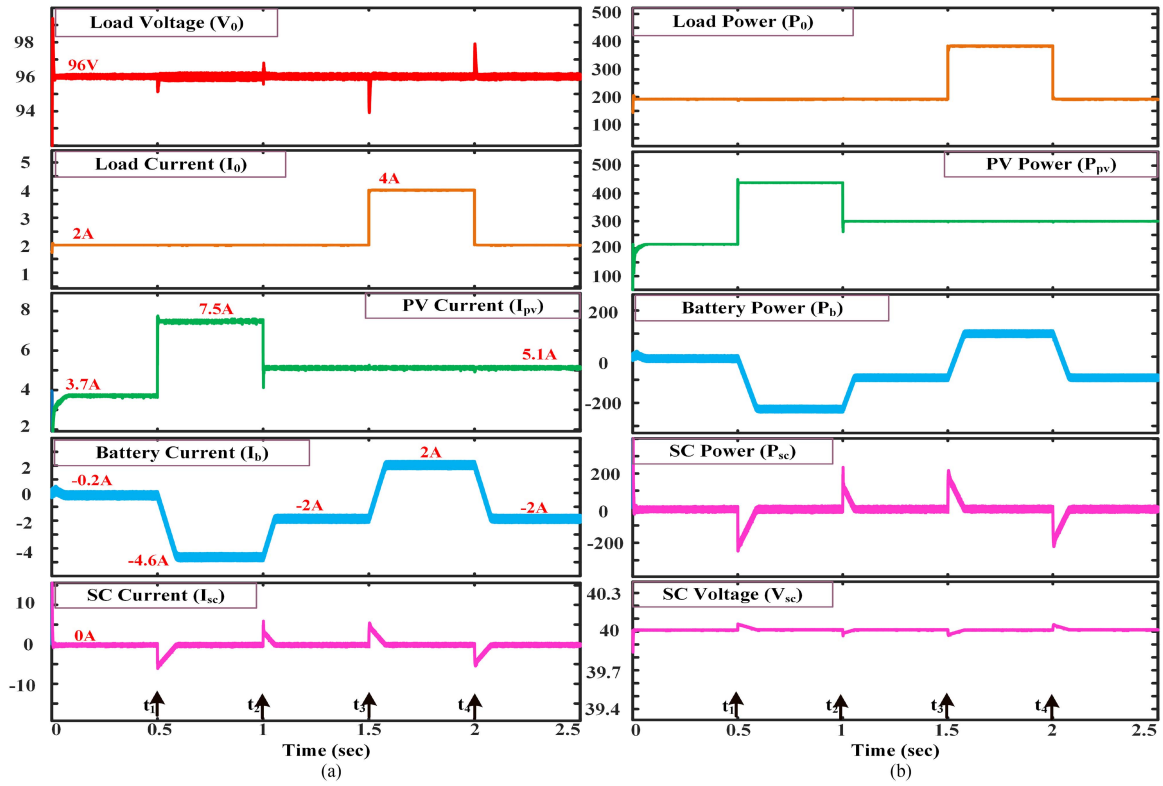

Fig. 5. Simulation results. (a) System parameters under different source and load variation; load voltage, load current, PV current, battery current, SC current; (b) power supplied, dissipated and absorbed by PV, load, battery, and SC, respectively.

TABLE II
COMPARISON BETWEEN PROPOSED CONTROLLER BASED ON RATE LIMITER (RL), PROPOSED CONTROLLER WITH LPF WITH OTHER CONTROL METHODS

Parameter	PI+ LPF [15]	PI+LPF [18]	MPC [21]	PI+SMC [25]	Proposed with LPF	proposed with RL
%Mp load disturbance	6–8%	4–5%	1–2 %	3.5–4.5 %	3.6–4.5%	1.5–2%
%Mp PV disturbance	2–3%	1.5–2.5%	0.5–1 %	1.5–2.5 %	1.5–2.5%	0.5–1%
Settling time (ms)	60–120	25–50	2–10	30–60	20–50	7–15
Execution time (μs)	25–30	25–30	50–55	25–30	25–30	10–15

discharge rate based on application. The hybrid controller with a rate limiter has less overshoot and settling time than the hybrid controller with a LPF, as shown in the dc bus voltage waveform. A comparative study with traditional PI, proposed + LPF and proposed + rate limiter are shown in Fig. 7(b). The traditional system requires 50 to 120 ms to reach the final state, while the proposed system with a LPF requires 20 to 50 ms to settle the dc bus voltage. The proposed system with a rate limiter only requires 7 to 12 ms to settle the oscillations in dc bus voltage. A detailed comparison of different topologies for HESS integrated dc microgrid is shown in Table II.

V. EXPERIMENTAL RESULTS

The isolated dc microgrid with PV source, battery, and the SC is shown in Fig. 8. The experimental setup consists of PV emulated dc source, Exide 12 V 7 Ah lead-acid battery, Maxwell BMOD0058 E016 B02 SC, IRF460 MOSFETS, sensor and driver circuit, dSPACE 1104 real-time controller, linear load, and other passive components. The system is designed for 100-W power, and the nominal power is 48 W. The output capacitor, PV converter inductor, battery converter inductor and SC inductor values are 470 μF, 2 mH, 2.3 mH, and 4.1 mH, respectively. The system operates with a dc bus voltage of 24 V. The system is verified under sudden variation in PV source and load. The hardware results are shown to evaluate the performance of the system.

A. System Operation Under Irradiance Variations

To analyze the performance of the proposed controller, disturbances are created at t_1, t_2, t_3, and t_4 similar to the scenarios presented in Section IV as shown in Fig. 9(a). The four traces represent dc bus voltage, PV current, battery current, and load current. The variation in incident PV panel irradiation is reflected as change in PV current as shown in t = t_1 and t = t_2. Initially, PV generation was sufficient to meet the load demand, and the battery current was almost zero. At t_1, the PV generation increases from 24 to 48 W. The excess power is absorbed by the battery and dc bus voltage regulated at 24 V. At t_2, the PV generation is reduced to 24 W and battery current reduces to nearly zero with minimal dc bus voltage variation. The slow change in battery current indicates that the SC is absorbing or supplying the transient power. An enlarged portion of PV variation is presented in Fig. 9(b). Initially, the battery current is almost zero, and

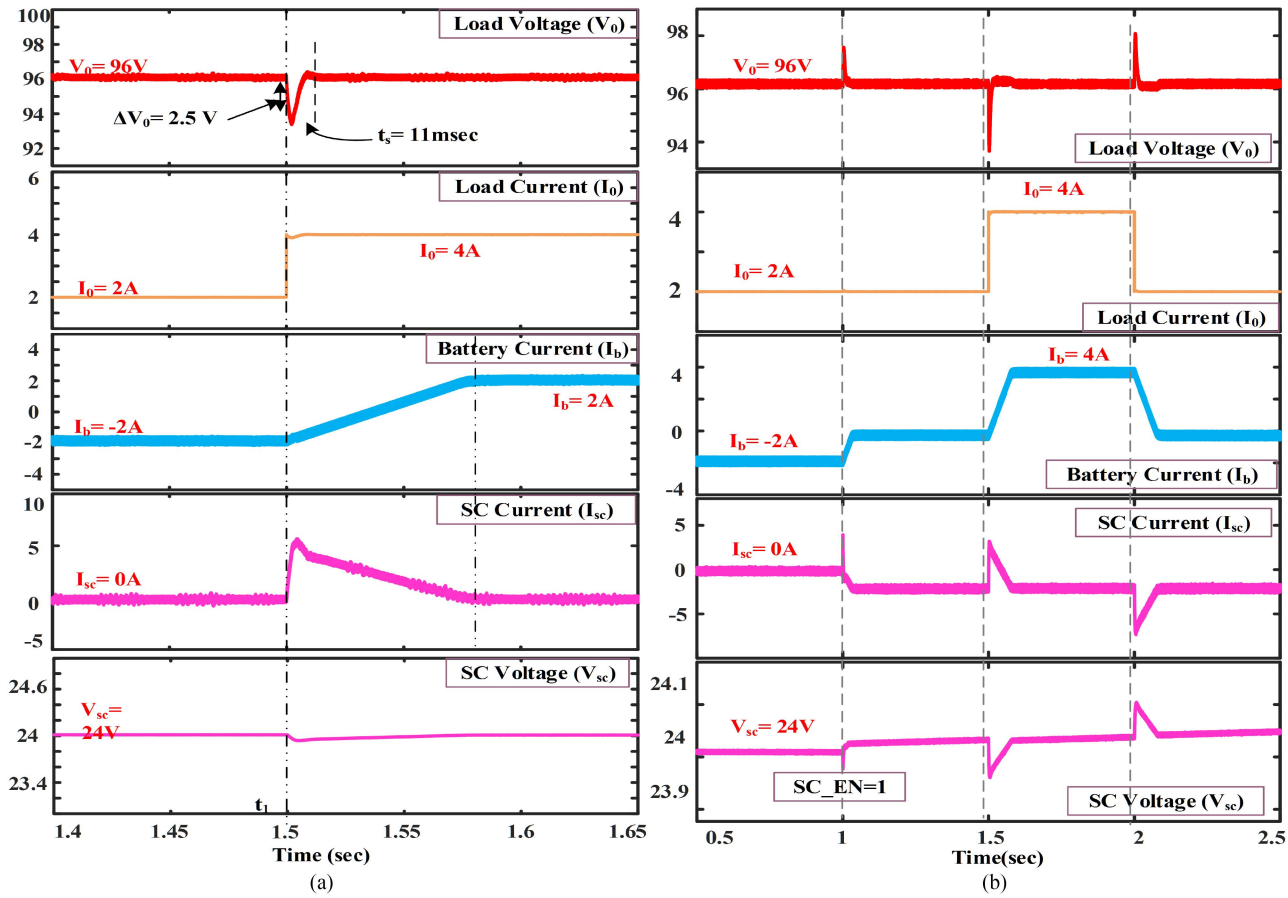

Fig. 6. Simulation results. (a) Enlarged view of Scenario-III with 50% SC voltage. (b) SSC charging under load disturbance.

PV meets the load demand. At the time of disturbance, the dc bus voltage and load current have a small oscillation and settle back to the original value. The battery current changes slowly according to the power sharing algorithm. The SC supplies the transient power, which helps to get faster system dynamics.

B. System Operation Under Load Variation

The load variation is applied by changing the connected load as shown in Fig. 9(a). At t_3, the load demand increases to 48 from 24 W and reduced to 24 W at t = t_4. Since the PV generation is constant, and the battery current varies to meet the excess power demand. The dc bus voltage is regulated constantly, and the battery current changes slowly compared to the change in load current. At t_3, the load demand increases by 1 A. The battery current increases to meet the additional power requirement. At t_4, the battery current reduces near 0 A since load demand is reduced to 1 A. For further understanding, the enlarged portion of battery and SC current sharing is illustrated in Fig. 10(a). Initially, the load is taking 2 A from PV and battery together. The enlarged portion shows the reduction in load current to 1 A. As a result, the battery current reduces to a new value based on the rate limiter algorithm. The SC absorbs the additional power created in the dc bus. Hence, SC current is negative in this operation.

C. System Operation Under SC Charging

To analyze the SC charging, excess PV generation and battery charging conditions are considered. Initially, the battery current is negative, and the SC current is almost zero. At $t = t_1$, the SC_EN made unity, thus, charging of SC is started. It can be seen from Fig. 10(b) that the battery current undergoes a smooth transition from negative current to the positive current during SC charging. The SC voltage slowly increases, and load voltage is maintained constant at 24 V. The combined system enables smooth SC charging without any disturbance in load voltage and battery current.

D. System Operation With Variation in "r"

The key feature of dynamic power sharing is controlling the battery discharge rate. A comparison is made for the analysis of battery and SC current sharing with different "r" values as shown in Fig. 11(a) and (b). The slope of battery current reduces as the "r" value increases from 0.0002 to 0.0005. It takes longer for the battery current to reach its final value when r = 0.0002 as shown in Fig. 11(a). The waveforms clearly show that the SC and battery share the total current during steady and transient states according to the power splitting strategy. Regardless of the rate limiter constant "r," the dc bus voltage is maintained at

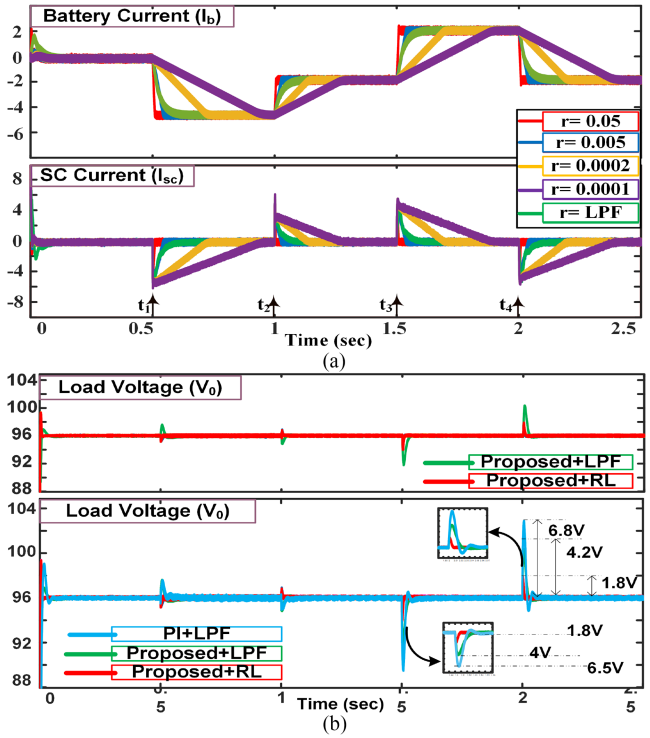

Fig. 7. Comparison of (a) effect of variation in "r" and LPF with cut-off frequency 31 rd/sec on battery and SC current, (b) corresponding load voltage and comparison of load voltage for Table II.

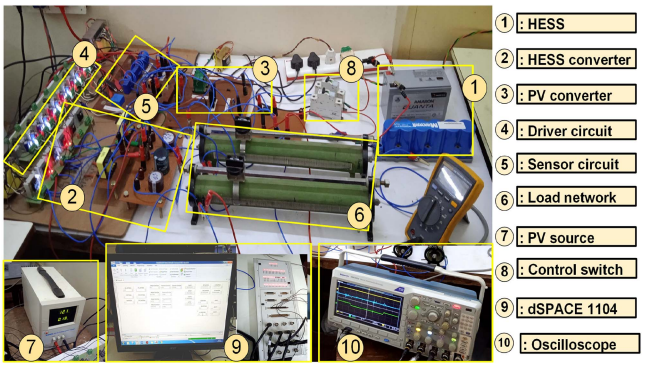

Fig. 8. Experimental setup developed for PV-dc microgrid.

24 V

$$\%\ \text{Maximum peak overshoot}\ (\%Mp) = \frac{V_{ref} - V_0}{V_0} X100\%. \tag{18}$$

E. Comparison With Previous Works

To further assess the performance of the hybrid control strategy, a comparison with prior studies is conducted and shown in Table II. The main parameter considered for comparison is percentage overshoot and settling time (t_s) taken by the dc bus voltage under various disturbances. The execution time is calculated using "turnaround time" in dSPCAE 1104. The percentage overshoot in dc bus voltage [9] is given by (18).

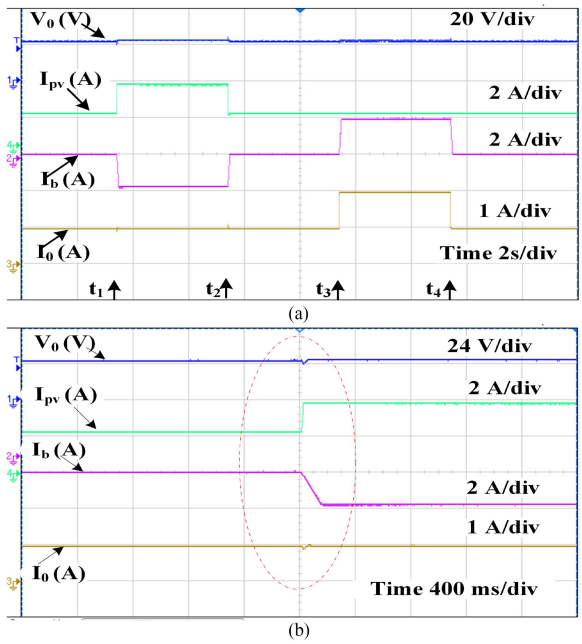

Fig. 9. Experimental results: (a) load voltage, load current, PV current, and battery current for different scenario, (b) current sharing between PV and battery during PV increment.

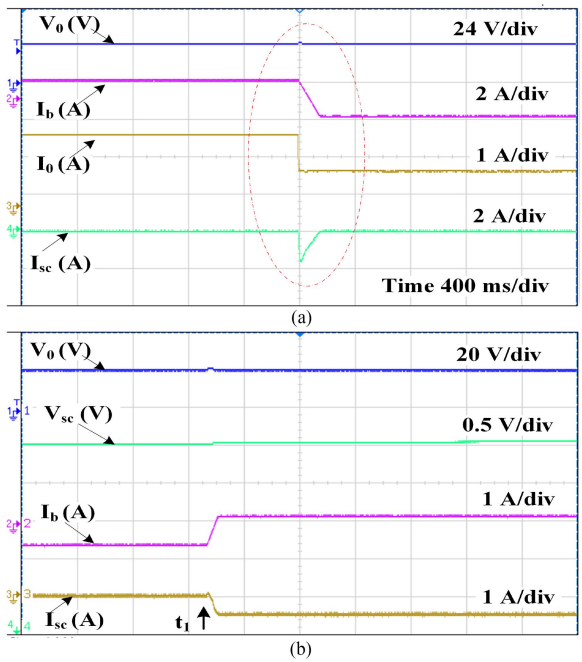

Fig. 10. Experimental results: (a) current sharing between battery and SC during load decrement, (b) charging of SC in excess power mode with SC_EN= 1.

Table II shows that the proposed hybrid control strategy has a lesser peak overshoot and settling time compared to the methods in [15], [18], and [25]. This implies better dc bus voltage regulation under different source and load variations. Also, the settling time of the proposed method is always less than 15 ms for the rate limiter method. This is because of

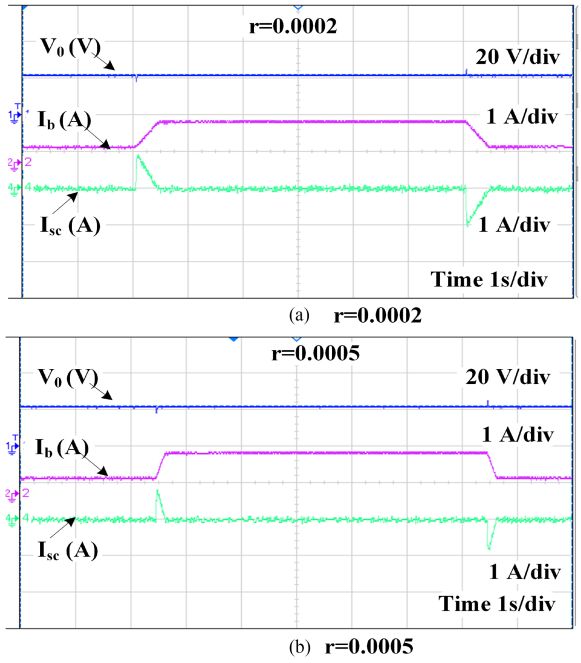

Fig. 11. Experimental results: dc bus voltage, battery current and SC current when (a) r= 0.0002, (b) r= 0.0005.

the reduction in system delay due to the combined action of rate limiter and internal predictive control for duty calculation. Though the comparison with the MPC controller shows slightly better dynamic performance due to optimization in duty selection, the proposed method has significantly less execution time, reducing the computational effort. Compared to controller execution time, the proposed method has the least computational effort required. The proposed control strategy with a LPF shows better performance than the traditional method; however, the delay imposed by the filter increases the settling and execution time. To summarize, the proposed control reduces computational complexity and improves the dynamic performance of the HESS integrated dc microgrid.

VI Conclusion

This article has presented a dual loop hybrid control scheme by combining traditional PI and predictive control schemes to control the battery and SC in a PV-dc microgrid. The conventional PI-LPF based HESS control strategies experience slow dynamic response due to low order LPF. Furthermore, there is no specific method to select the LPF cut-off frequency to control battery charge-discharge rates. Hence, a hybrid control strategy with a discrete rate limiter power sharing scheme is introduced for HESS. Using a rate limiter for the power splitting scheme enables a systematic approach to include battery discharge rate. It helps to eliminate slow response and the nonlinear nature of the LPF. The simulation study shows that the proposed method minimizes peak overshoot below 2% and settling time below 15 ms with stabilized dc bus voltage. Furthermore, the variation analysis with rate limiter constant shows that battery charge-discharge rates can be regulated independently without affecting the system dynamics. The SC charging is enabled using SC_EN below 50% of SC voltage and verified. The experimental studies reveal that the results follow the simulation study. The hardware results show that dc bus voltage has fewer oscillations and controls power sharing between the battery and the SC. To sum up, the proposed HESS controller integrated dc microgrid is able to reduce the controller complexity and effectively tackles the following required objectives such as:

1) limiting the rate of change of battery current;
2) uninterruptible SC charging without affecting the dc bus voltage and battery dynamics;
3) ensuring that the battery is supplied only for the steady-state power demand and SC is supplying the transient period;
4) limiting dc bus voltage fluctuations with minimum variation.

References

[1] A. A. R. Mohamed, R. J. Best, X. A. Liu, and D. J. Morrow, "A comprehensive robust techno-economic analysis and sizing tool for the small-scale PV and BESS," *IEEE Trans. Energy Convers.*, vol. 37, no. 1, pp. 560–572, Mar. 2022.

[2] L. Chong et al., "Hybrid energy storage systems and control strategies for stand-alone renewable energy power systems," *Renewable Sustain. Energy Rev.* vol. 66, pp. 174–189, 2016.

[3] P. Mathew, S. Madichetty, and S. Mishra, "A multilevel distributed hybrid control scheme for islanded DC microgrids," in *IEEE Syst. J.*, vol. 13, no. 4, pp. 4200–4207, Dec. 2019, doi: 10.1109/JSYST.2019.2896927.

[4] C. R. Arunkumar, U. B. Manthati, and S. Punna, "Supercapacitor voltage based power sharing and energy management strategy for hybrid energy storage system," *J. Energy Storage* vol. 50, 2022, Art. no. 104232.

[5] M. Li, L. Wang, Y. Wang, and Z. Chen, "Sizing optimization and energy management strategy for hybrid energy storage system using multiobjective optimization and random forests," in *IEEE Trans. Power Electron.*, vol. 36, no. 10, pp. 11421–11430, Oct. 2021, doi: 10.1109/TPEL.2021.3070393.

[6] Q. Xu, J. Xiao, X. Hu, P. Wang, and M. Y. Lee, "A decentralized power management strategy for hybrid energy storage system with autonomous bus voltage restoration and state-of-charge recovery," *IEEE Trans. Ind. Electron.*, vol. 64, no. 9, pp. 7098–7108, Sep. 2017, doi: 10.1109/TIE.2017.2686303.

[7] D. Alvaro, R. Arranz, and J. A. Aguado, "Sizing and operation of hybrid energy storage systems to perform ramp-rate control in PV power plants," *Int. J. Elect. Power Energy Syst.*, vol. 107, pp. 589–596, 2019.

[8] P. Srinivas, U. B. Manthati, and C. R. Arunkumar, "Modeling, analysis, and design of novel control scheme for two-input bidirectional DC-DC converter for HESS in DC microgrid applications," *Int. Trans. Elect. Energy Syst.*, vol. 31, 2021, Art. no. e12774.

[9] M. Ghiasi, "Detailed study, multi-objective optimization, and design of an AC-DC smart microgrid with hybrid renewable energy resources," *Energy*, vol. 169, pp. 496–507, 2019.

[10] E. Naderi, B. K. C., M. Ansari, and A. Asrari, "Experimental validation of a hybrid storage framework to cope with fluctuating power of hybrid renewable energy-based systems," *IEEE Trans. Energy Convers.*, vol. 36, no. 3, pp. 1991–2001, Sep. 2021, doi: 10.1109/TEC.2021.3058550.

[11] M. Asensio, G. Magallán, G. Amaya, and C. De Angelo, "Efficiency and performance analysis of battery-ultracapacitor based semi-active hybrid energy systems for electric vehicles," *IEEE Latin America Trans.*, vol. 16, no. 10, pp. 2581–2590, Oct. 2018, doi: 10.1109/TLA.2018.8795138.

[12] C. R. Arunkumar and U. B. Manthati, "Design and small signal modelling of battery-supercapacitor HESS for DC microgrid," *Proc. IEEE Region 10 Conf.*, 2019, pp. 2216–2221, doi: 10.1109/TENCON.2019.8929544.

[13] Z. Wang, P. Wang, W. Jiang, and P. Wang, "A decentralized automatic load power allocation strategy for hybrid energy storage system," *IEEE Trans. Energy Convers.*, vol. 36, no. 3, pp. 2227–2238, Sep. 2021, doi: 10.1109/TEC.2020.3038476.

[14] M. C. Joshi, S. Samanta, and G. Srungavarapu, "Frequency sharing based control of battery/ultracapacitor hybrid energy system in the presence of delay," *IEEE Trans. Veh. Technol*, vol. 68, no. 11, pp. 10571–10584, Nov. 2019, doi: 10.1109/TVT.2019.2941395.

[15] W. Jing et al., "A comprehensive study of battery-supercapacitor hybrid energy storage system for standalone PV power system in rural electrification," *Appl. Energy*, vol. 224, pp. 340–356, 2018.
[16] N. R. Tummuru, M. K. Mishra, and S. Srinivas, "Dynamic energy management of renewable grid integrated hybrid energy storage system," *IEEE Trans. Ind. Electron.*, vol. 62, no. 12, pp. 7728–7737, Dec. 2015, doi: 10.1109/TIE.2015.2455063.
[17] U. Manandhar, N. R. Tummuru, S. K. Kollimalla, A. Ukil, G. H. Beng, and K. Chaudhari, "Validation of faster joint control strategy for battery- and supercapacitor-based energy storage system," *IEEE Trans. Ind. Electron.*, vol. 65, no. 4, pp. 3286–3295, Apr. 2018, doi: 10.1109/TIE.2017.2750622.
[18] S. K. Kollimalla, M. K. Mishra, and N. L. Narasamma, "Design and analysis of novel control strategy for battery and supercapacitor storage system," *IEEE Trans. Sustain. Energy*, vol. 5, no. 4, pp. 1137–1144, Oct. 2014, doi: 10.1109/TSTE.2014.2336896.
[19] S. Kotra and M. K. Mishra, "A supervisory power management system for a hybrid microgrid with HESS," *IEEE Trans. Ind. Electron.*, vol. 64, no. 5, pp. 3640–3649, May 2017.
[20] P. Lin, P. Wang, J. Xiao, J. Wang, C. Jin, and Y. Tang, "An integral droop for transient power allocation and output impedance shaping of hybrid energy storage system in DC microgrid," *IEEE Trans. Power Electron.*, vol. 33, no. 7, pp. 6262–6277, Jul. 2018, doi: 10.1109/TPEL.2017.2741262.
[21] S. Chen, Q. Yang, J. Zhou, and X. Chen, "A model predictive control method for hybrid energy storage systems," *CSEE J. Power Energy Syst.*, vol. 7, no. 2, pp. 329–338, Mar. 2021, doi: 10.17775/CSEEJPES.2019.01960.
[22] B. Wang, U. Manandhar, X. Zhang, H. B. Gooi, and A. Ukil, "Deadbeat control for hybrid energy storage systems in DC microgrids," *IEEE Trans. Sustain. Energy*, vol. 10, no. 4, pp. 1867–1877, Oct. 2019, doi: 10.1109/TSTE.2018.2873801.
[23] Y. Hu, C. Chen, T. He, J. He, X. Guan, and B. Yang, "Proactive power management scheme for hybrid electric storage system in EVs: An MPC method," *IEEE Trans. Intell. Transp. Syst.*, vol. 21, no. 12, pp. 5246–5257, Dec. 2020, doi: 10.1109/TITS.2019.2952678.
[24] X. Zhang, B. Wang, D. Gamage, and A. Ukil, "Model predictive and iterative learning control based hybrid control method for hybrid energy storage system," in *IEEE Trans. Sustain. Energy*, vol. 12, no. 4, pp. 2146–2158, Oct. 2021.
[25] P. Singh and J. S. Lather, "Dynamic current sharing, voltage and SOC regulation for HESS based DC microgrid using CPISMC technique," *J. Energy Storage*, vol. 30, 2020, Art. no. 101509.
[26] M. Dehghani, M. Ghiasi, M. GhasemiGarpachi, T. Niknam, A. Kavousi-Fard, and H. Shirazi, "Stabilization of DC/DC converter with constant power load using exact feedback linearization method based on backstepping sliding mode control and nonlinear disturbance observer," in *Proc. 12th Power Electron., Drive Syst., Technol. Conf.*, 2021, pp. 1–6, doi: 10.1109/PEDSTC52094.2021.9405916.
[27] R. Bhosale and V. Agarwal, "Fuzzy logic control of the ultracapacitor interface for enhanced transient response and voltage stability of a DC microgrid," *IEEE Trans. Ind Appl.*, vol. 55, no. 1, pp. 712–720, Jan./Feb. 2019, doi: 10.1109/TIA.2018.2870349.
[28] S. Sinha and P. Bajpai, "Power management of hybrid energy storage system in a standalone DC microgrid," *J. Energy Storage*, vol. 30, 2020, Art. no. 101523.
[29] B. R. Ravada and N. R. Tummuru, "Control of a supercapacitor-battery-PV based stand-alone DC-microgrid," *IEEE Trans. Energy Convers.*, vol. 35, no. 3, pp. 1268–1277, Sep. 2020, doi: 10.1109/TEC.2020.2982425.
[30] C. Shah et al., "Review of dynamic and transient modeling of power electronic converters for converter dominated power systems," *IEEE Access*, vol. 9, pp. 82094–82117, 2021, doi: 10.1109/ACCESS.2021.3086420.
[31] R. W. Erickson and D. Maksimovic, *Fundamentals of Power Electronics*, Berlin, Germany: Springer, 2017.

Arunkumar Chirayarukil Raveendran received the B. Tech degree in electrical and electronics engineering and the M.Tech degree in power electronics and control from Mahatma Gandhi University, Kottayam, Kerala, in 2013 and 2016, respectively. He is currently working toward the doctoral program with the National Institute of Technology-Warangal, Telangana, India.

His research interests include dc microgrids, hybrid energy storage systems, and dc–dc converters.

Udaya Bhasker Manthati (Member, IEEE) was born in 1980. He received the B.Tech. degree in electrical and electronics engineering from JNTU Hyderabad, India and the M.E. degree in power electronics and drives from the Sathyabama Institute of Science and Technology, Chennai, India, in 2003 and 2006, respectively, and the Ph.D. degree in electrical engineering from the Technical University of Catalonia, Barcelona, Spain, in 2011.

Since 2022, he has been an Associate Professor with the Department of Electrical Engineering, National Institute of Technology-Warangal, Telangana, India. From 2011 to 2021, he was an Assistant Professor with Manipal University Jaipur, Rajasthan, India, and the National Institute of Technology-Warangal. From 2007 to 2011, he was a Research Assistant with the Technical University of Catalonia, Barcelona, Spain. He has authored or coauthored for various national and international reputed journals and conferences. He has written two book chapters of international repute on energy storage systems. He is at present supervising M.Tech. and Ph.D. thesis in the domain of hybrid energy storage technologies and digital control. His research interests include dc–dc converters, power electronics to micro grid and smart grid technologies, energy storage systems, digital control, and synchrotron power supplies.

Dr. Manthati was a recipient of the Synchrotron Light Laboratory-UPC fellowship during 2007-2010.